Structural Relationships, Crystal Chemistry and Anion Substitution Processes for M(III)X$_3$ Systems of the Lanthanides and Actinides

J. M. HASCHKE

Department of Chemistry, University of Michigan, Ann Arbor, Michigan 48104

An examination of data for lanthanide and actinide phases with UCl$_3$-type and PuBr$_3$-type M(III)X$_3$ structures has shown that these systems are conveniently described by alternating layers of $[MX_2]_n^{n+}$ and $[X]_n^{n-}$. The relationships between the UCl$_3$- and PuBr$_3$-type structures are described and expanded to include a variety of anion substitution systems, M(III)X$_{3-x}$Y$_x$. The two different types of $[MX_2]_n^{n+}$ layers observed in these systems are consistent with the existence of a novel structural unit, $[M_2X_4]^{2+}$. The effects of radius ratio constraints and layering mechanisms on the phase equilibria and anionic substitution processes, polymorphism and crystal growth in the MX$_{3-x}$Y$_x$ systems are discussed.

Introduction

The ideas presented in this paper have resulted from an examination of the structures of several lanthanide(III) and actinide(III) systems containing monovalent anions. The original impetus for the investigation was the observation of similar structural features for a variety of anion substitution phases in the lanthanide + hydroxide + nitrate systems (*1, 2*). Nitrate substitution phases, M(OH)$_{3-x}$ (NO$_3$)$_x$ have been characterized for $x = 0.25$–0.5 and $x = 1$; like the terminal ($x = 0$) member, M(OH)$_3$, all polymorphic forms of the mixed anion phases have lattices with monoclinic or higher symmetry. The most peculiar feature is that the twofold or a higher symmetry axis in these systems is extremely short and varies linearly with M^{3+} radius from approximately 4.0 Å at La to 3.5 Å at Lu. Examination of structural data for other M(OH)$_{3-x}$ Y$_x$ systems, e.g. Y = F$^-$ (*3*), Cl$^-$ (*4–8*), and even O^{-2} (*9–11*), and for unsubstituted MX$_3$ systems, e.g., X = OH$^-$ (*9, 12–14*), Cl$^-$ (*12, 14, 15*), Br$^-$ (*12, 14–16*) and I$^-$ (*12, 14, 17*), reveals similar lattices with short twofold axes. A somewhat

less obvious feature of these phases is that the axial vectors normal to the short axis are frequently 6–7 Å in length, or some multiple of that distance.

After the essential structural relationships had been defined, it was observed that phase equilibria, anionic substitution processes and crystal growth habits of the MX$_{3-x}$Y$_x$ systems can be elucidated by consideration of structural features. An effort to develop these ideas has also been made.

Structure Descriptions

MX$_3$ Structures

The hexagonal UCl$_3$(YOH$_3$)-type structure. The structure, which has been classified as both Y(OH)$_3$-type (*12*) and UCl$_3$-type (*14*), is conveniently described (Fig. 1a) by alternating triangular-shaped columns of $[MX_3]_n$ normal to the projection plane. These give trigonal-prismatic coordination of M^{3+} by X$^-$. Adjacent columns are staggered by one-half unit along the projection axis, and a ninefold coordination of M^{3+} arises from the six anions in the trigonal prismatic arrangement
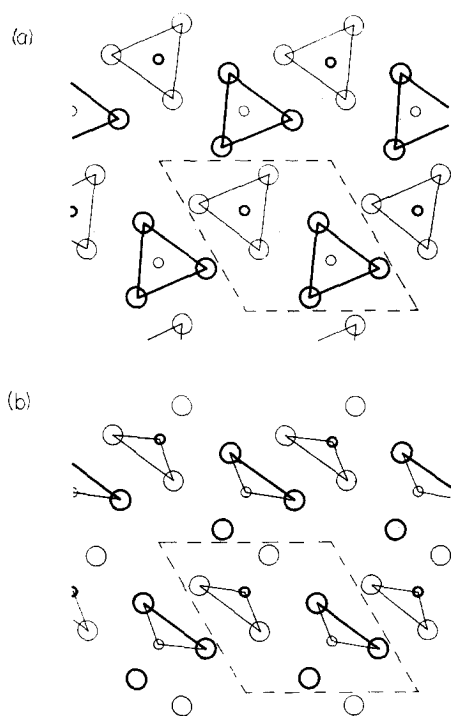
FIG. 1. Projection of the hexagonal UCl$_3$- or Y(OH)$_3$-type MX$_3$ structure on the (001) plane. (a) shows the structure as alternating triangular columns of MX$_3$, and (b) shows the structure as alternating layers of [MX$_2$]$_n^{n+}$ and [X]$_n^{n-}$. (Large and small circles represent X$^-$ and M^{3+}, respectively, light circles are at $z = \frac{1}{4}$, and heavy circles are at $z = \frac{3}{4}$. The data are those of Y(OH)$_3$ (13), with $P6_3/m$, $a = 6.24$, $c = 3.53$ Å, $Z = 2$.)
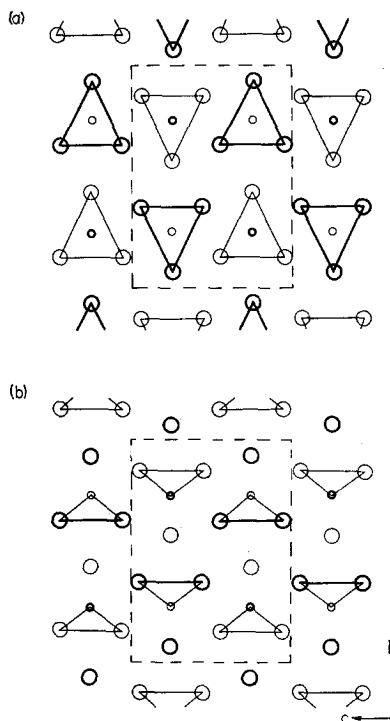
FIG. 2. Projection of the orthorhombic PuBr$_3$-type MX$_3$ structure on the (100) plane. (a) shows the structure as alternating triangular columns of MX$_3$, and (b) shows the structure as alternating layers of [MX$_2$]$_n^{n+}$ and [X]$_n^{n-}$. (Large and small circles represent X$^-$ and M^{3+} ions, respectively, light circles are at $x = \frac{1}{4}$, and heavy circles are at $x = 0$. In the standard setting, the PuBr$_3$ structure (15) is $Cmcm$ with $a = 4.10$, $b = 12.64$, $c = 9.14$ Å, $Z = 4$.)

and from three anions which belong to neighboring columns and occupy the rectangular faces of the trigonal prism.

Figure 1b indicates that UCl$_3$-type phases can also be described as layered structures defined by alternating infinite layers of [MX$_2$]$_n^{n+}$ and [X]$_n^{n-}$. The [MX$_2$]$_n^{n+}$ layers are composed of triangular-shaped fragments of the [MX$_3$]$_n$ columns described above, and therefore, also alternate up and down by a half unit along the projection axis. It should be emphasized that all anions in the structure are equivalent, and three identical choices for layering are possible.

The orthorhombic PuBr$_3$-type structure. Like UCl$_3$, the PuBr$_3$-type structure (Fig. 2) (12, 14, 15) may also be defined by alternating

columns of [MX$_3$]$_n$; however, comparison of Figs 1 and 2 shows that the triangular columns are oriented differently in the two structures. In PuBr$_3$, the packing of columns is appropriate for ninefold coordination of the metal, but as Wells (14) has previously noted, the anions occupying the trigonal prism faces normal to [010] are essentially non-bonded because of their distance (approximately 4.0 Å in PuBr$_3$) from the metal.

Examination of Fig. 2b shows that the PuBr$_3$-type structures may also be described by alternating layers of [MX$_2$]$_n^{n+}$ and [X]$_n^{n+}$. The [MX$_2$]$_n^{n+}$ layers are composed of triangular shaped fragments like those in UCl$_3$; however, their arrangement within the layers

are different. It has been noted above that the anions in $PuBr_3$ are inequivalent, and consequently the layering array in Fig. 2b is unique with all of the nonbonded anions appearing in the $[X]_n^{n-}$ layers. Although layering in this system has been noted previously (14), only the layers of $[MX_3]_n$ composition have been described.

$MX_{3-x}Y_x$ Structures

The monoclinic $Y(OH)_2Cl$-type structures. The projection in Fig. 3 clearly shows that the $Y(OH)_2Cl$ structure (5, 7) is defined by alternating layers of $[M(OH)_2]_n^{n+}$ and $[Cl]_n^{n-}$. This structure type has been reported for the lanthanide dihydroxide monochlorides (18) and may exist for the dihydroxide mononitrates (2); however, some uncertainty exists concerning the space group for the chloride systems (8). An eightfold coordination of the metal arises from six hydroxides in the $[M(X)_2]_n^{n+}$ layer and from two chlorides in the $[Y]_n^{n-}$ layer. Comparison of Fig. 3 with Fig. 1b shows that the arrangement of $M(X)_2^+$

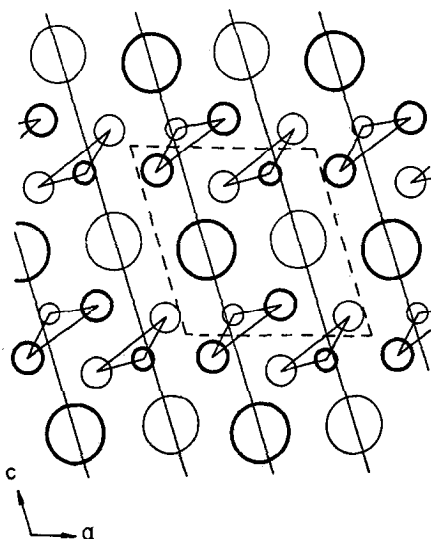FIG. 3. Projection of the monoclinic $Y(OH)_2Cl$-type MX_2Y structure on the (010) plane. (Large, medium and small circles represent Y^-, X^- and M^{3+} ions, respectively; light circles are at $y = \frac{1}{4}$, and heavy circles are $y = \frac{3}{4}$. The $Y(OH)_2Cl$ structure (5) is $P2_1/m$ with $a = 6.14$, $b = 3.62$, $c = 6.60$ Å, $\beta = 107°$, $Z = 2$.)

fragments in the hydroxide layers is similar to that observed in the $[MX_2]_n^{n+}$ layers of the UCl_3-type phases. The solid lines parallel to [001] in Fig. 3 are related to polymorphism which is discussed subsequently.

The orthorhombic $La(OH)_2NO_3$-type substructure. The high temperature modification of $La(OH)_2NO_3$ (2) shows a pronounced substructure–superstructure relationship. The superstructure has not been defined, but the substructure (Cmcm, $a = 4.076$, $b = 13.070$, $c = 7.208$ Å, $Z = 4$) is a $PuBr_3$-type lattice (19) containing alternate layers of $[M(OH)_2]_n^{n+}$ and $[NO_3]_n^{n-}$. A projection of the structure closely resembles that in Fig. 2b; a ninefold metal coordination arises from six hydroxides in the $[MX_2]_n^{n+}$ layer and from the oxides of three nitrates in adjacent anion layers.

Structure Relationships

The $[M_2X_4]^{2+}$ Groups as a Structural Unit

Examination of the $[MX_2]_n^{n+}$ layers observed for a variety of MX_3 and $MX_{3-x}Y_x$ structures shows the existence of only two types of layers, those found in the UCl_3- and $PuBr_3$-type structures. It has been noted above that both types of $[MX_2]_n^{n+}$ layers have sixfold coordination within the layers, but differ in the internal arrangements of their triangular $[MX_2]^+$ fragments. An obvious conclusion is that the triangular $[MX_2]^+$ fragments, which form infinite columns normal to the projection plane, are the basic structural units of the layers. However, a closer examination of the two types of layers show that both contain paired $[MX_2]^+$ fragments which are displaced by one-half unit along the projection axis and interrelated by a twofold screw. These $[M_2X_4]^{2+}$ groups stack with formation of infinite $[M_2X_4]_n^{n+}$ columns normal to the projection planes in Figs 1–3 and appear to be the basic structural units of the $[MX_2]_n^{n+}$ layers.

The existence of $[MX_2]_n^{n+}$ structural units is substantiated by an examination of the relationship between the UCl_3- and $PuBr_3$-type layers in Fig. 4. If one begins with a unit cell layer of UCl_3 structure (Fig. 4a) and retains only the $[MX_2]_n^{n+}$ layer (Fig. 4b), a simple
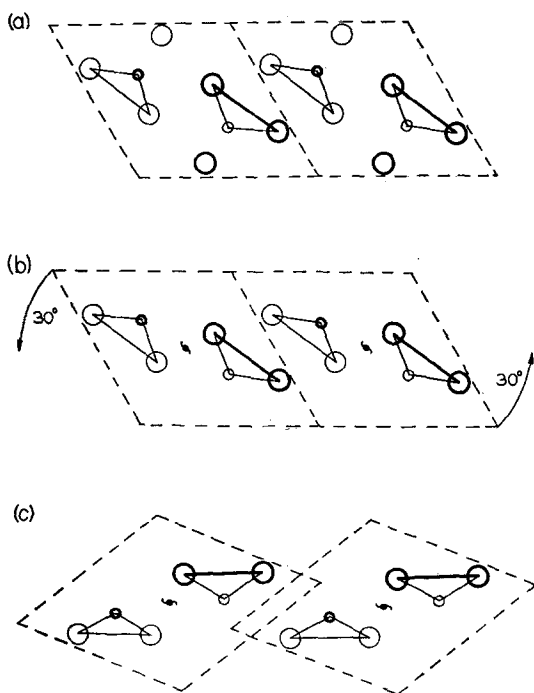
FIG. 4. Relationship between the $[MX_2]_n^{n+}$ layers in UCl$_3$- and PuBr$_3$-type structures. (a) and (b) show the projection of a UCl$_3$-type structure (cf. Fig. 1) with and without the adjacent anion layers, respectively. (b) indicates one set of operations which converts the UCl$_3$-type layer into the PuBr$_3$-type layer in (c).

30° rotation of the $[M_2X_4]^{2+}$ units about their twofold axes and a slight expansion of the layer transforms the UCl$_3$-type layer into a PuBr$_3$-type layer (Fig. 4c). The interconversion is also achieved by appropriate arrangement of the hexagonal UCl$_3$ cells with their (110) planes parallel to the layer plane. In the UCl$_3$-type layers (Fig. 4b), sixfold coordination of M is attained by occupying the rectangular face of each triangular $[MX_2]^+$ fragment by anions of adjacent $[MX_2]^+$ fragments in the layer. In the layers of PuBr$_3$-type structures (Fig. 4c), sixfold intralayer coordination is achieved by direct coordination of the metal from the side opposite the rectangular face. Therefore, the UCl$_3$- and PuBr$_3$-type layers are conveniently described as "mutually back shared" and "mutually front shared" arrays of $[M_2X_4]^{2+}$ units, respectively. Since the coordination within

each $[M_2X_4]^{2+}$ group is front-shared, the PuBr$_3$-type layers exhibit only front sharing. For UCl$_3$, the coordination alternates between front and back sharing.

The $[M_2X_4]^{2+}$ group is a rather unusual structural unit, but its existence accounts for the similar structural features of the MX$_3$ and MX$_{3-x}$Y$_x$ systems. The short twofold or higher symmetry axes, i.e. the projection axes in Figs. 1–3, arise because of the short repeat distance of this group normal to the projection plane. Since the $[MX_2]_n^{n+}$ layers are composed of ordered columns of $[M_2X_4]_n^{n+}$ which have twofold axes, a minimum twofold axis is found in the layers. The layers always contain a second lattice vector orthogonal to the twofold axis; this repeat distance is determined by the length of the $[M_2X_4]^{2+}$ unit, and for UCl$_3$-type layers gives rise to lattice vectors which are multiples of approximately 6 Å.

The Relationship of UCl$_3$- and PuBr$_3$-Type Structures

The existence of a simple relationship between the $[MX_2]_n^{n+}$ layers of UCl$_3$ and PuBr$_3$ suggest that a similar relationship exists between the two structure types. If unit cells of hexagonal UCl$_3$-type structure are arranged with parallel (110) planes as shown by the dashed lines in Fig. 5, an orthorhombic PuBr$_3$-type array is generated. It should be noted that adjacent layers of MX$_3$ composition defined by strings of hexagonal cells parallel to the $[MX_2]_n^{n+}$ layers are dissimilar and may be interchanged by a half-unit translation along the projection axis.

Figures 4 and 5 demonstrate that a primary difference between the UCl$_3$- and PuBr$_3$-type structures is their mode of intralayer coordination, and the known structures of MX$_3$ compounds of the lanthanides and actinides are consistent with radius ratio constraints on mutual front sharing and mutual back sharing by $[M_2X_4]^{2+}$ groups. Back sharing and the resultant UCl$_3$-type layers is obviously favoured by low anion to cation ratios; UCl$_3$-type structures are observed for X$^-$/M^{3+} ≤ 1.93 (16). At higher ratios the anion–anion repulsion inherent in back
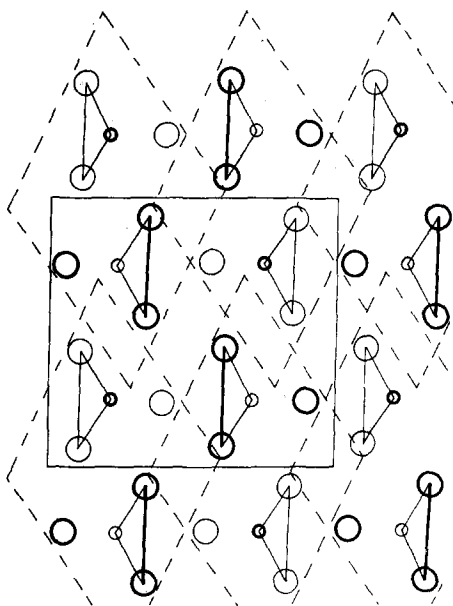
FIG. 5. Relationship of the UCl₃- and PuBr₃-type structures. (The data for the UCl₃-type structure are those given for Fig. 1.)

FIG. 6. Relationship of the UCl₃- and Y(OH)₂Cl-type structures. (The data for the UCl₃ type structure are those given for Fig. 1.)

sharing is avoided by front sharing, i.e., transition to PuBr₃-type layers and eight (or nine) fold coordination. The radius ratio range for stability of PuBr₃-type structures varies markedly for different anions, but at $X^-/M^{3+} > 2.0$–2.2, six coordinate YCl₃ (or AlCl₃)- or BiI₃ (or FeCl₃)-type structures are observed (16). These materials have some structural similarities with the UCl₃- and PuBr₃-type systems, but neither appears to be based on layers derived from $[M_2X_4]^{2+}$ structural units.

The Relationship of UCl₃- and Y(OH)₂Cl-Type Structures

In the above description of the Y(OH)₂Cl-type structures, it was noted that the $[MX_2]_n^{n+}$ layers are of the UCl₃-type; a simple relationship of the nine-coordinate UCl₃- and eight-coordinate Y(OH)₂Cl-type structures is expected. Figure 6 indicates that they may be related by a one-step translational shear mechanism. If adjacent unit cell layers of UCl₃-type structure are translated by $a/4$ parallel to [100], the coordination is reduced from nine to eight. The resulting monoclinic

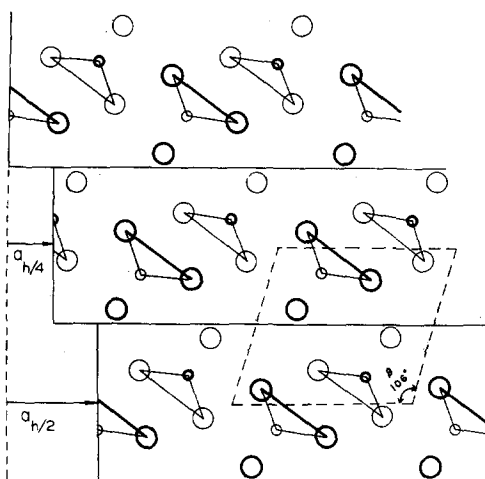lattice has $\beta \simeq 106°$; that observed for Y(OH)₂Cl is 107° (4). For this system, OH^-/Y^{3+} is suitable for the formation of back-shared UCl₃-type $[MX_2]_n^{n+}$ layers, but the larger Cl⁻ obviously does not pack well in the nine-coordinate structure and the more favorable eight-coordinate structure is adopted.

Phase Equilibria and Crystal Growth

Isomorphous Anion Substitution

Radius ratio constraints in the MX₃ systems drastically limit the number of monovalent anions which are expected to form isomorphous substitution phases; however, systems such as UCl₃-type lanthanide hydroxide fluorides phases have been described (3). Across the lanthanide series, the homogeneity ranges of the $M(OH)_{3-x}F_x$ vary regularly from $1.0 \leqslant x \leqslant 1.1$ at La to $1.5 \leqslant x \leqslant 2$ at Yb. Random isomorphous substitution has been assumed, and a structure refinement based on the intensities of powder X-ray data is consistent with this interpretation (3); however, the observed homogeneity ranges suggest preferential occupancy of the layers. The La system shows a narrow miscibility range near $M(OH)_2F$, and the maximum composition for the heavier ele-

ments is $M(OH)F_2$. Radius ratio constraints favor the formation of $[M(OH)_2]_n^{n+}$ and $[MF_2]_n^{n+}$ layers for the lighter and heavier lanthanides, respectively.

Layering and Anion Substitution

The description of UCl₃- and PuBr₃-type phases with alternating layers of $[MX_2]_n^{n+}$ and $[X]_n^{n-}$ provide a more general mechanism for substitution of monovalent anions in these systems. The $Y(OH)_2Cl$ and $La(OH)_2NO_3$ systems provide excellent examples. If the X^-/M^{3+} value is suitable for the formation of $[MX_2]_n^{n+}$ layers, occupancy of a fraction of the $[X]_n^{n-}$ layers by Y^- anions provides a mechanism for the formation of substitution series such as $Ln(OH)_{3-x}(NO_3)_x$ (2). Although the $x = 0$ member is trivial ($X = Y = OH^-$), the $x = 0.5$ and $x = 1$ compositions may be attained by occupancy of every second and every anion layer with NO_3^-, respectively. If the ionic radii of X^- and Y^- differ noticeably, a random distribution of X^- and Y^- in the anion layers is not expected at $x = 0.5$, nor are additional series members, i.e., $x > 1$, anticipated. In the hydrothermal hydroxide nitrate systems, a maximum value of $x = 1$ is observed (2); substitution of NO_3^- into the $[Ln(OH)_2]_n^{n+}$ layers apparently destroys the network backbone of the structures and leads to solubility in the aqueous phase.

Structures of the $MX_{3-x}Y_x$ systems with $x \simeq 0.5$ have not been determined, but the presence of short axes and parameters which are multiples 6–7 Å suggest that these materials have structures based on $[MX_2]_n^{n+}$ layers. The lattice parameters (2) are not the simple twofold multiples which are required by alternate occupance of the anion layers by X^- and Y^-. The large lattice parameters and the substructure–superstructure relationships of these systems (1) suggest that these materials might be best described by alternating slabs of $M(X)_3$ and $M(X)_2Y$.

The lanthanide oxide hydroxide systems (9) incorporate an interesting combination of isomorphous and layering substitution mechanisms and demonstrate an interesting relationship between the $[MX_2]_n^{n+}$ and the previously described $[MO]_n^{n+}$ systems (20).

Radius ratio constraints for substitution into the UCl₃-type trihydroxides are satisfied by O^{2-}, and charge balance requirements are met by formation of vacancies in the anion layers. At the MOOH composition, the anion layers are completely vacant and the resultant $[MOOH]_n$ layers collapse to give a sevenfold coordination of the metals as shown in Fig. 7.

The uniqueness of the YOOH-type structure is immediately obvious. The back shared UCl₃-type $[MOOH]_n$ layers lie parallel to the (110) planes as indicated by the solid diagonal lines in upper part of Fig. 7. Front shared PuBr₃-type layers parallel to the (001) planes also define the structure and indicate that the same collapsed structure results from the elimination of anion layers from either the UCl₃- or PuBr₃-type structure. Finally, the structure is described by layers of $[MO]_n^{n+}$ and $[OH]_n^{n-}$ (20) which lie parallel to the (100) planes. The O^{2-} ions, which are readily
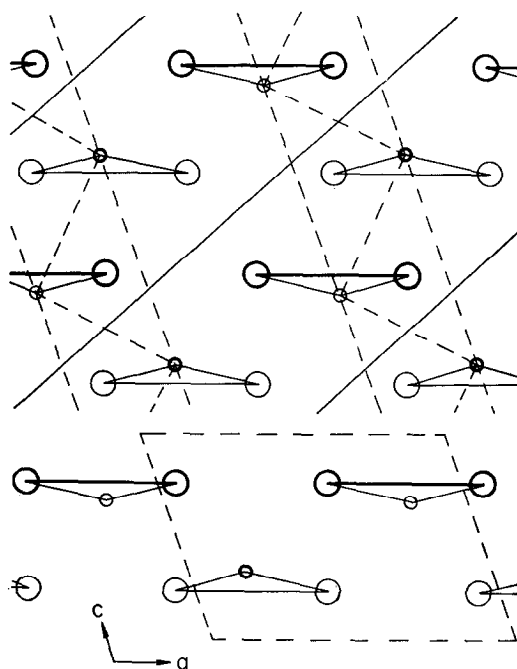

FIG. 7. Projection of the monoclinic YOOH-type structure on the (010) plane. (Large and small circles represent anions and cations, respectively; light circles are at $y = \frac{1}{4}$ and heavy circles are at $y = \frac{3}{4}$. The data are those of HoOOH (10) with $P2_1/m$, $a = 5.96$, $b = 3.64$, $c = 4.31$ Å, $\beta = 109.1°$, $Z = 2$.)

identified by their shorter metal to anion distances, occupy the mutually back shared positions of the UCl_3-type layers, and each is tetrahedrally coordinated by four metals as indicated by the dashed triangular projections in the upper part of Fig. 7. These edge shared tetrahedra form MOCl-type $[MO]_n^{n+}$ layers normal to the projection plane and alternate with the $[OH]_n^{n-}$ layers.

Structural similarities of the UCl_3-type lanthanide trihydroxides and the monoclinic oxide hydroxides have been noted previously by Klevtsova and Klevtsov (*11*), who have shown which atoms are removed from $M(OH)_3$ during dehydration to MOOH. With the present structural interpretation of MX_3 phases, further elucidation of this process is possible. Occupancy of mutually back shared positions by O^{2-}, and retention of the mutually front shared positions by OH^- during dehydration are consistent with radius ratio predictions and with the apparent stability of the $[M_2X_4]^{2+}$ unit. Association of two oxide ions in mutually back shared positions of a UCl_3-type trihydroxide produces a nucleation site for growth of the layered MOOH structure shown in Fig. 7.

Intergrowth, Polymorphism and Twinning

In the $MX_{3-x}Y_x$ systems with similar layered structures for different x values, the presence of ordered and random intergrowth is anticipated. Ordered intergrowth of layers are implied by the above discussion of structures of the $x = 0.5$ hydroxide nitrates. The presence of identical $[M(X_2)]_n^{n+}$ layers in slabs or domains of MX_3 and MX_2Y composition provides an obvious mechanism for coherent intergrowth. Random intergrowth of $M(OH)_2F$ and $M(F)_2OH$ domains may also be the origin of the observed miscibility ranges of the UCl_3-type hydroxide fluorides.

Several types of polymorphism are also anticipated. In the above discussion, two forms of $La(OH)_2NO_3$ have been described. Both consist of $[La(OH)_2]_n^{n+}$ and $[NO_3]_n^{n-}$ layers. Their essential difference is that the cation layers in the monoclinic form appear to be the back shared UCl_3-type while those in the orthorhombic form are the front shared $PuBr_3$-type. Monoclinic and ortho-

rhombic forms of $M(OH)_2Cl$ have also been described and discussed (*7*). Comparison of the lattice parameters for these phases (*8*) suggest that they might have the same relationship as the hydroxide nitrates; however, the orthorhombic $M(OH)_2Cl$ phases have primitive lattices which arise from different layering effects. The projection of the $Y(OH)_2Cl$ structure in Fig. 8 shows that the chloride layers act as pivotal points for intergrowth of adjacent $[M(OH)_2]_n^{n+}$ layers which are mirror images. Comparison of Fig. 8 with the projection of the monoclinic structure in Fig. 3 shows that the orthorhombic form results from intercellular twinning of the monoclinic form and exhibits the herring-bone pattern characteristic of such relationships (*21*).

The coherent intergrowth of layers or slabs with the compositions MX_3 and MX_2Y suggests possibilities of polytypism and twinning and provides a plausible explanation for

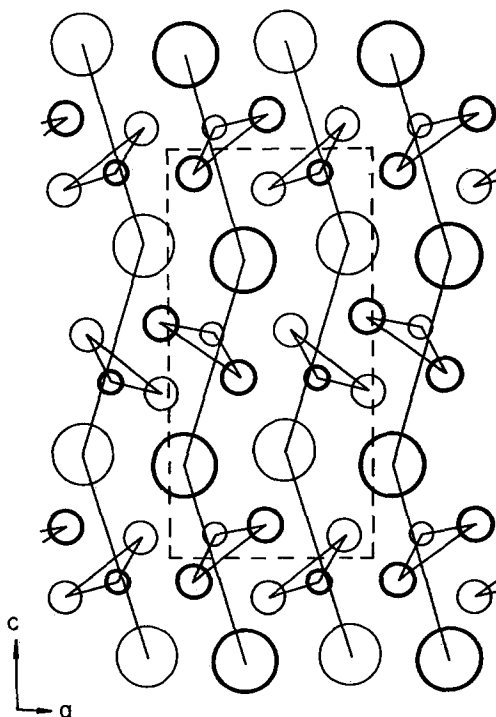Fig. 8. Projection of the orthorhombic $Y(OH)_2Cl$ structure on the (010) plane. (The identification key is that for Fig. 3. The $Y(OH)_2Cl$ structure (*4*) is *Pcmn* with $a = 6.21$, $b = 3.62$, $c = 12.56$ Å, $Z = 4$.)

the existence and properties of the intermediate $MX_{3-x}Y_x$ phases with $0.25 < x < 0.5$ (2). If the structures of these compositions are based on alternation of slabs of MX_3 and MX_2Y, polytypism from long range ordering of slabs may be observed. Compositions are easily altered by variations in slab width; however, such composition effects could also arise from twinning like that of the hypothetical UCl_3-type $M_6X_{16}Y_2$ ($MX_{2.67}Y_{0.33}$) system shown in Fig. 9. The layer directions are altered by the coherent intergrowth of sheets of triangular MX_3 normal to the projection plane as indicated by the dashed lines. These twinning layers generate a herring-bone pattern and drastically alter the bulk composition of the phase. Diffraction data for a large number of $M(OH)_{3-x}(NO_3)_x$ crystals from bulk compositions near that of the hypothetical phase indicate a high level
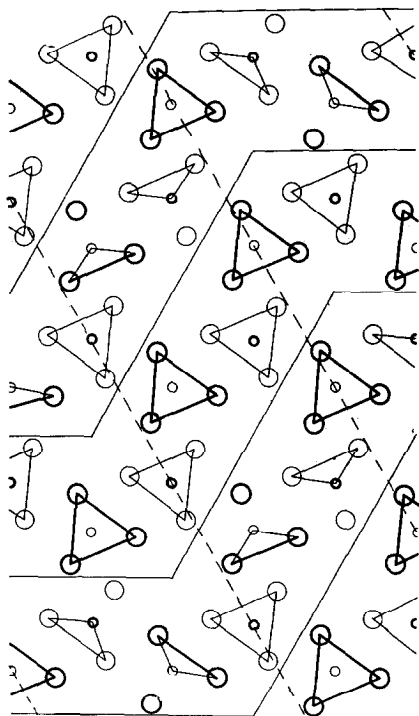
of disorder; however, further work is necessary for verification of these proposals.

An interesting type of coherent intergrowth is observed in the structure of $Y_3O(OH)_5Cl_2$ (22), which may be described by alternating layers of $[Y_3O(OH)_4]_n^{2n+}$ and $[OHCl]_n^{2n-}$. Examination of the cation layers shows that they consist of alternating columns of back shared $[Y_2(OH)_4]_n^{n+}$ and $[YO]_n^{n+}$. As in the YOOH-type structure, the short repeat distance of metals in the $[M_2(OH)_4]_n^{n+}$ columns corresponds to the edge length of MO_4 tetrahedra employed for description of lanthanide oxide anion phases (20). The $[Y_2(OH)_4]_n^{n+}$ columns share metals with the $[YO]_n^{n+}$ columns to give tetrahedral coordination of O^{-2}. Such coherent intergrowth of $[M_2(OH)_4]_n^{n+}$ and $[MO]_n^{n+}$ columns suggests the possibility of preparing homologous series oxide hydroxide anion phases with the general formula $[MO]_n[M_2(OH)_4]_m[Y]_{n+m}$.

Crystal Growth Habits

An examination of the morphologies of $MX_{3-x}Y_x$ crystals shows two types of growth habits, thin rectangular platelets and needles. In all cases, the rapid growth direction is colinear with the short crystallographic vector, and in the case of platelets, the rapid growth directions are those defined by the $[MX_2]_n^{n+}$ layers. Addition to $[MX_2]_n^{n+}$ columns is always rapid and extension of the cation layers is also facile in many systems; however, the addition of new layers is slow. These growth habits are consistent with a structural interpretation based on the existence of $[MX_2]_n^{n+}$ network layers.

FIG. 9. Projection of a hypothetical $M_6X_{16}Y_2$ structure derived from a UCl_3-type and regular twinning planes of MX_3 composition. (The identification key for UCl_3-type structures is given in Fig. 1. All X^- ions are connected to adjacent X^- or M^{3+} ions by lines.)

Conclusions

The present description of MX_3 and $MX_{3-x}Y_x$ systems of the lanthanides and actinides is similar to that developed by Caro for metal oxide and oxide anion systems (20). In both cases the parent binary systems may be defined by alternating layers of metal + anion and anion; in the ternary systems the anion layers are occupied by a second anion. The metal + anion layers, $[MX_2]_n^{n+}$ and $[MO]_n^{n+}$, are formed from unusual structural units, $[M_2X_4]^{2+}$ and OM_4

tetrahedra, which may be arranged to give two different types of layers. These parallel descriptions have been shown to merge coherently in MOOH- and $M_3O(OH)_5Cl_2$-type structures.

An understanding of the structural relationships of MX_3 systems correlates the crystal chemistry for a large fraction of lanthanide and actinide hydroxides, chlorides, bromides, and iodides and suggest possibilities for further study. For example, the preparation of mixed halides such as MF_2Cl and MCl_2Br should be possible, and their characterization should provide equilibrium data and structural information for further elucidation of MX_3 and $MX_{3-x}Y_x$ systems.

Acknowledgment

References

1. J. M. HASCHKE AND L. EYRING, *Inorg. Chem.* **10**, 2267 (1971).

2. J. M. HASCHKE, *Inorg. Chem.* **13**, 1812 (1974).

3. A. MARBEUF, G. DEMAZEAU, S. TURRELL, P. HAGENMULLER, J. DEROUET, AND P. CARO, *J. Solid State Chem.* **3**, 637 (1971).

4. P. V. KLEVTSOV, R. F. KLEVTSOVA, AND L. P. SHEINA, *Zh. Strukt. Khim.* **6**, 469 (1965); *J. Struct. Chem.* **6**, 449 (1965).

5. R. F. KLEVTSOVA AND P. V. KLEVTSOV, *Zh. Strukt. Khim.* **7**, 556 (1966); *J. Struct. Chem.* **7**, 524 (1966).

6. R. F. KLEVTSOVA AND P. V. KLEVTSOV, *Dokl. Akad. Nauk SSSR* **162**, 1049 (1965).

7. K. DORNBERGER-SCHIFF AND R. F. KLEVTSOVA, *Acta Crystallogr.* **22**, 435 (1967).

8. F. L. CARTER AND S. LEVINSON, *Inorg. Chem.* **8**, 2788 (1969).

9. G. BRAUER, "Progress in the Science and Technology of the Rare Earths" (L. Eyring, Ed.), Vol. 3, Ch. 9, Pergamon Press, New York, 1968.

10. A. N. CHRISTENSEN, *Acta Chem. Scand.* **19**, 1391 (1965).

11. R. F. KLEVTSOVA AND P. V. KLEVTSOV, *Zh. Strukt. Khim.* **5**, 860 (1964); *J. Struct. Chem.* **5**, 795 (1964).

12. R. W. G. WYCKOFF, "Crystal Structures," Vol. 2, Ch. VB, Wiley, New York, 1964.

13. K. SCHUBERT AND A. SELTZ, *Z. Naturforsch.* **1**, 321 (1946).

14. A. F. WELLS, "Structural Inorganic Chemistry," 3rd Ed., Ch. VIII and XXVI, Oxford University Press, London, 1962.

15. W. H. ZACHARIASEN, *Acta Crystallogr.* **1**, 265 (1948).

16. D. BROWN, S. FLETCHER, AND D. G. HOLAH, *J. Chem. Soc. A*, **1968**, 1889 (1968).

17. L. B. ASPREY, T. K. KEENAN, AND F. H. KRUSE, *Inorg. Chem.* **3**, 1137 (1964).

18. R. F. KLEVTSOVA AND L. A. GLENSKAYA, *Zh. Str. Khim.* **10**, 494 (1969); *J. Str. Chem.* **10**, 408 (1969)

19. L. R. WYLES, T. A. DELINE, J. M. HASCHKE, AND D. R. PEACOR, "Proceedings of the Eleventh Rare Earth Research Conference", USAEC CONF-741002-P2, USAEC Technical Information Center, Oakridge, Tenn., p 550, 1974.

20. P. E. CARO, *J. Less-Common Metals* **16**, 367 (1968).

21. S. ANDERSSON AND B. G. HYDE, *J. Solid State Chem.* **9**, 92 (1974).

22. R. F. KLEVTSOVA, L. P. KOZEEVA, AND P. V. KLEVTSOV, *Izv. Akad. Nauk SSSR, Neorgan. Materialy* **3**, 1430 (1967); *Inorg. Mater.* **3**, 1247 (1967).